# Explainable Visual Anomaly Detection via Concept Bottleneck Models

Arianna Stropeni<sup>1</sup>, Valentina Zaccaria<sup>1</sup>, Francesco Borsatti<sup>1</sup>, Davide Dalle Pezze<sup>1</sup>, Manuel Barusco<sup>1</sup>, Gian Antonio Susto<sup>1</sup>

<sup>1</sup>University of Padova, Italy

arianna.stropeni@studenti.unipd.it, valentina.zaccaria.1@phd.unipd.it, francesco.borsatti.1@phd.unipd.it, davide.dallepezze@unipd.it, manuel.barusco@phd.unipd.it, gianantonio.susto@unipd.it

Abstract—In recent years, Visual Anomaly Detection (VAD) has gained significant attention due to its ability to identify anomalous images using only normal images during training. Many VAD models work without supervision but are still able to provide visual explanations by highlighting the anomalous regions within an image. However, although these visual explanations can be helpful, they lack a direct and semantically meaningful interpretation for users. To address this limitation, we propose extending Concept Bottleneck Models (CBMs) to the VAD setting. By learning meaningful concepts, the network can provide human-interpretable descriptions of anomalies, offering a novel and more insightful way to explain them. Our contributions are threefold: (i) we develop a Concept Dataset to support research on CBMs for VAD; (ii) we improve the CBM architecture to generate both concept-based and visual explanations, bridging semantic and localization interpretability; and (iii) we introduce a pipeline for synthesizing artificial anomalies, preserving the VAD paradigm of minimizing dependence on rare anomalous samples. Our approach, Concept-Aware Visual Anomaly Detection (CON-VAD), achieves performance comparable to classic VAD methods while providing richer, concept-driven explanations that enhance interpretability and trust in VAD systems.

Index Terms—Visual Anomaly Detection, Explainability, Concept Bottleneck Model

# I. Introduction

Visual Anomaly Detection (VAD) is a computer vision task that aims to identify both normal and anomalous images, while also highlighting the pixels responsible for the anomaly. VAD has applications in various fields, including, but not limited to, manufacturing, medicine, and surveillance [1], [2], [3]. However, collecting an annotated dataset for training VAD models in a supervised way is costly and time-consuming, especially in the manufacturing domain, when the dataset must comprise several images with a wide range of defect types. Because of this, in recent years, many VAD models have been developed and trained based on an unsupervised paradigm, which requires the training set to be made up only of normal images. Although VAD models can produce anomaly segmentation masks and thus provide interpretable results, it is questionable whether these visual insights are sufficient, as they fail to deliver a human-understandable description of the anomaly and the problematic image as a whole. In this work, we address the lack of interpretability in VAD models by considering a different VAD paradigm based on Concept Bottleneck Models (CBMs) [4]. Incorporating CBM models

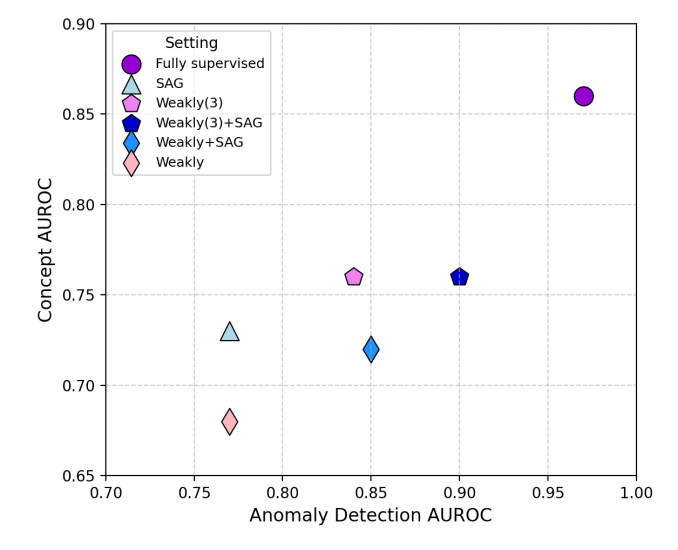


Fig. 1: In a fully supervised setting, CONVAD achieves performance comparable to established VAD models while additionally offering interpretable, concept-based explanations. Additionally, it shows competitive performance also in settings where anomalous images are scarce.

into the VAD framework enables it to providing not only image/pixel-level labels but also a series of concepts that can be used by the final user to understand model predictions and enhance the decision-making process. In addition, thanks to CBMs, the users can perform interventions on the intermediate features (concepts), aiding the model in making the final correct prediction, enabling seamless **human-machine collaboration**, which would not be possible in the classic VAD models.

This work, to the best of our knowledge, is the first to test the adaptation of CBMs to the Visual Anomaly Detection scenario. This adaptation is not straightforward, and a series of challenges have been tackled:

(i) CBM models require a Concept Dataset for training, where each sample is annotated with a set of concepts from a predefined concept vocabulary. However, no such dataset currently exists for VAD. Therefore, to adress this gap, we propose an automated pipeline for extracting meaningful con-

cepts and annotating state-of-the-art industrial datasets with them, leveraging the capabilities of Vision Language Models (VLMs).

- (ii) Unsupervised VAD approaches have the advantage of providing a pixel-level visualization of the area of the anomaly, which standard CBMs do not, since **they are limited to sample-level predictions**. We thus extend the CBM architecture to provide not only concept-based explanations but also visual explanations using the student-teacher paradigm alongside the concept extractor.
- (iii) Current state-of-the-art VAD models assume to have only normal images during training, but **CBMs need both normal** and anomalous images to be trained. We introduce a pipeline for generating synthetic anomalies, enabling effective concept learning while minimizing dependence on rare and difficult-to-acquire anomalous samples.

The rest of the paper is organized as follows: Sec. II provides relevant VAD literature, while Sec. III explains in detail the CBM architecture and training methodologies. Then, Sec. IV shows our method, Concept-Aware VAD (CONVAD), which is based on the CBM models and adapts them for the VAD setting, solving the previously discussed problems. Sec. V outlines the experimental setting with implementation details and considered VAD scenarios. Sec. VI discusses the results. Finally, Sec. VII suggests directions for future work.

#### II. RELATED WORK

A significant amount of research has been conducted in the Visual Anomaly Detection (VAD) domain in recent years, leading to the development of numerous VAD models. Most VAD methods can be broadly categorized into the following three groups:

- 1. Feature-based Methods: these approaches rely on representations extracted from pre-trained neural networks. By leveraging the rich semantic and structural information encoded in these features, anomalies can be detected as deviations from normal patterns. Some well-known feature-based methods include PatchCore [5], STFPM [6], FastFlow [7] and PaDiM [8].
- 2. Reconstruction-based Methods: reconstruction-based methods operate under the assumption that models trained solely on normal data will struggle to accurately reconstruct anomalous regions. During inference, reconstruction errors highlight potential anomalies. Examples of such methods include AnoGAN [9], f-AnoGAN [10], and UniAD [11]. A downside compared with feature-based models is the need to train a generative model, which can be computationally expensive and resource-intensive.
- **3. Synthetic Anomaly Methods:** these methods augment the original dataset by generating synthetic anomalies, enabling the model to learn explicit representations of anomalous patterns. Early approaches relied on simple, non-realistic augmentations, such as CutPaste [12] and DRAEM [13], which randomly modify normal images to simulate defects. More recent approaches leverage advanced generative models to produce highly realistic anomalies, improving both robustness and detection performance [14].

However, although these methods can generate visual explanations in the form of anomaly maps, they are limited, as they cannot provide human-understandable explanations using natural language or semantic concepts. While advanced VLMs [15], [16], [17] can generate natural language explanations, their high memory requirements and slow inference speeds often make them impractical for many real-world applications, especially those that require lightweight models deployed close to the environment. Therefore, a more efficient and intuitive approach to providing human-understandable explanations is through the use of concepts. Some works try to use concept-based explanations for out-of-distribution (OOD) in the computer vision domain, such as [18], [19], and [20]. However, they fail to reflect realistic scenarios like VAD, as they typically treat entire classes as anomalous, simplifying the problem and reducing its practical relevance. Another work, called LogicAD, focuses on detecting logical anomalies and leverages a VLM for predictions. However, the work is more focused on exploring strategies to improve the reasoning capabilities of VLMs, rather than providing a straightforward interpretation of the anomaly. Moreover, their approach is highly resource-intensive, both in terms of memory and computation, since they rely on a VLM during inference. Hence, to the best of our knowledge, we present the first study exploring the use of CBMs for the VAD problem, evaluating their effectiveness in this context. In particular, as highlighted in Sec. I, we address many challenges in adapting CBMs to the VAD setting.

# III. CONCEPT BOTTLENECK MODELS

A CBM [4] is an interpretable neural architecture designed to make predictions via an intermediate set of human-interpretable concepts. Among the advantages of CBMs is their usefulness in edge scenarios: unlike large VLMs, CBMs can operate with very limited memory and extremely fast inference speeds while still providing human-understandable explanations. This makes them particularly suitable for deployment in resource-constrained or real-time environments, where interpretability and speed are crucial.

Formally, let  $\mathbf{x} \in \mathcal{X}$  be the input,  $\mathbf{c} \in \mathcal{C}$  represent a vector of k concepts, and  $y \in \mathcal{Y}$  denote the target label. A CBM consists of two functions: a concept extractor  $g: \mathcal{X} \to \mathcal{C}$ , which maps the input  $\mathbf{x}$  to a predicted concept vector  $\hat{\mathbf{c}} = g(\mathbf{x})$ , and a label predictor  $f: \mathcal{C} \to \mathcal{Y}$ , which maps the predicted concepts  $\hat{\mathbf{c}}$  to the final output  $\hat{y} = f(\hat{\mathbf{c}})$ .

The CBM is then the composition  $\hat{y} = f(g(\mathbf{x}))$ . The intermediate concept layer acts as a bottleneck, constraining the downstream prediction  $\hat{y}$  to depend on  $\mathbf{x}$  entirely through the concept predictions. This improves the interpretability of the model final output, but also enables test-time intervention, as discussed below.

Standard CBMs require supervised learning, i.e., access to ground-truth triplets  $\{\mathbf{x}^i, \mathbf{c}^i, y^i\}_{i=1}^m$  must be provided during training. In our VAD setting, the input  $\mathbf{x}$  is a raw image and the target label y is binary, with y=1 if the image contains an anomaly and y=0 otherwise. We consider the true concepts to be only binary, namely  $\mathcal{C}=\{0,1\}^k$ .

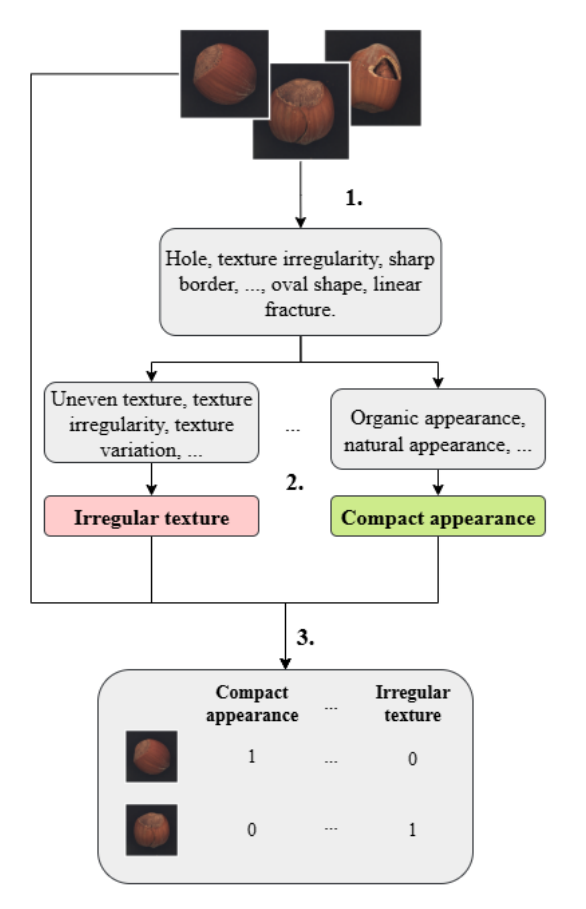


Fig. 2: Pipeline for creating the Concept Dataset through concept annotation of a VLM.

# A. CBM Training

A CBM can be trained using three different modalities, which are compared in our experiments:

• **Independent training**: the concept extractor is trained to predict concepts from inputs:

$$\hat{g} = \arg\min_{g} \sum_{i,j} \mathcal{L}_{C_j}(g_j(\mathbf{x}^i), c_j^i), \tag{1}$$

where  $\mathcal{L}_{C_j}$  denotes the loss associated with the j-th concept prediction. Separately, the label predictor is trained using the ground-truth concept vectors  $\mathbf{c}$  as input:

$$\hat{f} = \arg\min_{f} \sum_{i} \mathcal{L}_{Y}(f(\mathbf{c}^{i}), y^{i})$$
 (2)

where  $\mathcal{L}_Y$  is the loss for the downstream label prediction. Note that, during deployment,  $\hat{\mathbf{c}}$  takes as input the predicted concept vector  $\hat{\mathbf{c}} = \hat{g}(\mathbf{x})$  rather than the true ones. This may lead to a shift between the training and inference input distributions, potentially degrading performance.

• Sequential training: first, g is trained as in the independent setting, in Eq. 1. Then, f is trained using as input the predicted concepts  $\hat{\mathbf{c}} = \hat{g}(\mathbf{x})$  rather than the true ones.

 Joint training: g and f are trained jointly, end-to-end, optimizing the combined loss:

$$\hat{f}, \hat{g} = \arg\min_{f,g} \sum_{i} \mathcal{L}_{Y}(f(g(\mathbf{x}^{i})), y^{i}) + \lambda \sum_{i,j} \mathcal{L}_{C_{j}}(g_{j}(\mathbf{x}^{i}), c_{j}^{i}),$$
(3)

where  $\lambda$  balances the concept and label prediction terms. In the sequential and joint setting, predicted concepts  $g_j(\mathbf{x^i})$  are not binary as the ground-truth, but they are logits and the model f takes these logit values as input.

#### B. CBM Test-time Interventions

A key property of CBMs is their ability to support test-time interventions. When a user or domain expert supervising the system identifies one or more incorrectly predicted concepts, they can manually correct them by setting  $\hat{c}_j = c_j$ . The resulting correct concept vector  $\tilde{\mathbf{c}}$  is then fed into the label predictor f, which produces an updated (and ideally more accurate) output  $\tilde{y} = f(\tilde{\mathbf{c}})$ . In sequentially and jointly trained models, where f receives concept logits rather than binary values, interventions correct the corresponding logits by setting them to the 5th or 95th percentile of the training logit distribution, preventing extreme values.

This mechanism allows the expert to influence the final prediction without retraining the model, leading to an increased downstream task performance. This intervention capability is unique to CBMs, due to their bottleneck structure.

## IV. METHODOLOGY

# A. Concept Dataset Pipeline

One of the main challenges faced by Concept Bottleneck Models, which prevents their widespread adoption in several real-world applications, is the lack of datasets annotated with image concepts, which are unavailable in many domains, including VAD. Manually defining a list of attributes and checking their presence in each picture can be time-consuming and resource-intensive, especially in datasets of large sizes. Due to this reason, several efforts have been focused on devising a partially or fully automated pipeline for concept extraction, mainly leveraging the capabilities of VLMs. Among the most notable ones, we recall Label-free CBMs [21], LaBo [22] and VLG-CBMs [23].

The task at hand, however, differs significantly from those considered in previous works, which were typically centered on multiclass classification of natural images. Here, instead, the main task is binary, and the concepts that are useful to identify and describe an anomaly in an industrial scenario are highly domain-specialized and fine-grained. Furthermore, defective industrial images do not appear often in the training sets of VLMs, which are usually trained on datasets of natural images. Due to this reason, we devise an ad-hoc pipeline for concept extraction and propose a prompt specifically designed to detect anomalies that are typically overlooked by VLMs when generating image descriptions, resulting in concept extraction that is otherwise ineffective for VAD tasks.

The quality of the automatically annotated dataset will be evaluated against a ground-truth one, which was manually annotated, so that we can safely guarantee that employing VLM-extracted concepts does provide high-quality and reliable results (see Appendix).

Our procedure, shown in Fig. 2, can be summarized in the following steps: *context-aware list creation, grouping and filtering, and automatic dataset annotation*.

1. Context-aware list creation: A common aspect of all the algorithms for automated concept extraction is the creation of a concept list through the aid of an VLM, which is prompted to generate a list of features that are useful to recognize something as belonging to a class, as well as objects that are commonly seen around the main element of the image. This is usually done independently of the dataset, so no training image is passed to the model to be used as a reference. In our scenario, however, dataset-free annotations are not suitable due to several reasons: first, it is not possible to make a general list of industrial defects without including information about which objects are considered in the dataset, as anomalies are category-specific; second, even among the same category, datasets can heavily differ on which defects they choose to consider, and a predetermined list might not fully capture their variability; finally, the lack of a wide number of industrial images in the training datasets of LLMs might lead to either hallucinations or the failure to include some important anomalies.

To tackle the previous issues, we introduce a context-aware paradigm for the generation of a single concept list for each object category at hand. We consider a representative subset of the training set composed of 5% of the total number of images, making sure that all defect types are represented.

Let g denote the Vision-Language Model (VLM), x an input image, and pt a textual prompt. Using the VLM g, together with an image x and the prompt pt, our goal is to extract a set of meaningful concepts by directly injecting contextual understanding into the prompt, providing information related to the object category and the defect at hand, and by leveraging a Chain-of-Thought (CoT) prompting strategy [24], which involves breaking down a complex task into interpretable reasoning steps. Specifically, in our case, the prompt first asks the model to generate a natural language description of the image, and then to extract up to five semantic concepts from it. By constraining the model to extract concepts only from a visual description of the image, we avoid the risk that it focuses on non-visual attributes, and we reduce the risk of hallucinations.

Let  $X = \{x_i \in D \mid i = 1, ..., N\}$  be a subset of images sampled from the dataset D. For each image  $x_i$ , we define  $c_i = g(x_i, pt)$  as the set (or list) of concepts extracted by the VLM when conditioned on the prompt.

The complete collection of all extracted concepts can then be expressed as:

$$C = \{c_{ij} \mid i = 1, \dots, N; \ j = 1, \dots, |c_i|\},\$$

where  $c_{ij}$  denotes the j-th concept obtained from image  $x_i$ .

- **2. Grouping and filtering:** after creating the full list, it undergoes a process of automatic refinement, intending to group together semantically related concepts and exclude those that are not suitable for the downstream task. The process can be broken down into two subtasks:
- (i) **Concept grouping**: first, the full list is fed to the VLM, prompting it to group attributes that are morphologically and semantically related. We utilize few-shot learning to guide the VLM in its output by providing two examples of how the groups should look; this strategy has proven to increase the quality of the response [25]. This first step allows the number of concepts to be reduced from a few hundred to less than fifty attributes.
- (ii) **Concept filtering**: this step is for the removal of concepts that do not satisfy requirements that make them useful for the downstream task. We specifically follow the criteria and the procedure detailed in [21], which first suggests excluding concepts that are too similar to each other: in order to estimate such similarity, we encode the tokenized attributes to generate text features, using the text encoder ET from the CLIP ViT-B/32 text encoder [26], and then we compute the cosine similarity between each pair of concepts,  $c_i$  and  $c_j$ :

$$\cos(\mathrm{ET}(c_i), \mathrm{ET}(c_j)) = \frac{\mathrm{ET}(c_i) \cdot \mathrm{ET}(c_j)}{\|\mathrm{ET}(c_i)\| \|\mathrm{ET}(c_j)\|}$$
(4)

For each pair that has a similarity higher than 0.9, we exclude one of the two according to the following criteria: if one appears in another pair of high similarity, we exlude that one; otherwise, we randomly choose which one to discard.

3. Automatic dataset annotation The final step involves annotating each image with the concepts present in it. We focus on hard annotations that assign a binary label to each attribute depending on whether it is present in the selected image or not. Therefore, we query a VLM with a prompt that is still guided by the object category, the label, and the type of defect, similar to what was done during the creation of the concept list. The model is asked to inspect the image and the list of attributes and to return an object that associates a boolean variable to each concept according to its presence or absence, which will then be encoded in a binary label.

# B. CBM Adaptation for Visual Explanations

Classic VAD approaches have the advantage of providing a pixel-level visualization of the area of the anomaly, which standard CBMs do not. To add visual insights to the explanations provided by concepts, we devise a pipeline that makes use of the student-teacher paradigm [27]. Specifically, we treat the backbone employed for concept prediction as a teacher network that distills knowledge into a similar student network, randomly initialized and trained to match teacher features for the normal images. In this way, we effectively pair the textual interpretation provided by the CBM with a visualization of the area of the anomaly. A schematic illustration is provided in Fig. 3.

# C. Synthetic Anomaly Generation

In this study, synthetic anomalous images are created by modifying normal images using a text-to-image and image-

Category	STFPM	Fu	lly	Wea	ıkly	Weakly	y+SAG	SA	<b>G</b>
	I-AUC	C-AUC	I-AUC	C-AUC	I-AUC	C-AUC	I-AUC	C-AUC	I-AUC
Bottle	0.99	0.99	1.00	0.95	1.00	0.79	0.97	0.80	0.94
Cable	0.91	0.87	1.00	0.69	0.79	0.67	0.76	0.80	0.88
Capsule	0.69	0.92	0.98	0.55	0.61	0.56	0.63	0.52	0.52
Carpet	0.96	0.72	1.00	0.61	0.97	0.81	0.90	0.75	0.72
Grid	0.77	0.96	0.81	0.55	0.41	0.71	0.88	0.72	0.64
Hazelnut	0.92	0.95	1.00	0.85	0.99	0.85	0.99	0.89	0.99
Leather	0.99	0.85	1.00	0.72	0.94	0.72	0.98	0.80	0.90
Metal Nut	0.92	0.92	1.00	0.73	0.82	0.70	0.84	0.59	0.66
Pill	0.81	0.81	0.97	0.63	0.76	0.63	0.75	0.62	0.60
Screw	0.55	0.82	0.93	0.59	0.53	0.55	0.70	0.48	0.49
Tile	0.99	0.9	1.00	0.76	0.94	0.84	0.96	0.76	0.86
Toothbrush	0.84	0.92	0.80	0.82	0.47	0.75	0.77	0.61	0.56
Transistor	0.96	0.55	0.85	0.35	0.73	0.59	0.73	0.66	0.66
Wood	0.99	0.81	1.00	0.71	0.90	0.80	0.98	0.82	0.93
Zipper	0.90	0.92	1.00	0.70	0.69	0.82	0.95	0.70	0.68
Average	0.88	0.86	0.97	0.68	0.77	0.72	0.85	0.73	0.77

TABLE I: All models are trained on the complete set of non-defective images. Fully denotes training with 80% of the abnormal images in the original dataset. Weakly indicates one-shot training per defect type (dataset mean: 4.9 defect types per category). SAG refers to training augmented with synthetic anomalies. Weakly+SAG combines one-shot training per defect type with synthetic anomaly augmentation.

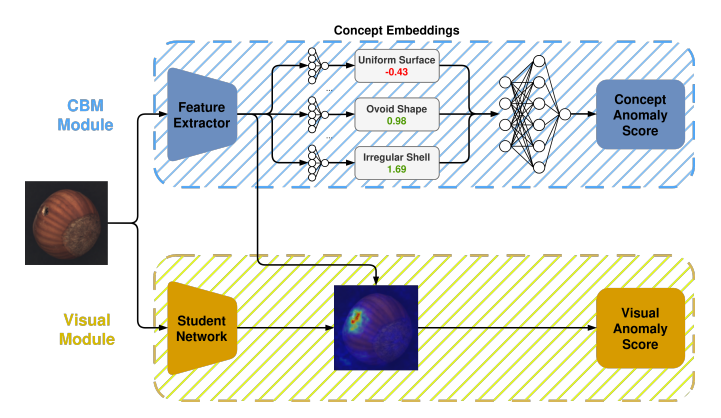


Fig. 3: CONVAD Architecture with the i) CBM Module and the ii) Vision Module.

editing system. Let  $\mathcal{G}_{\text{edit}}(\mathbf{x},p)$  denote the editing function, which takes  $\mathbf{x} \in \mathbb{R}^{H \times W \times 3}$  as input image and p that represents a textual prompt. Starting from a normal image  $\mathbf{x}_n$ , the generative procedure create an anomalous image  $\mathbf{x}_a = \mathcal{G}_{\text{edit}}(\mathbf{x}_n, p_a)$  where  $p_a$  includes the desired defect type and ensures consistency with the original image. The scope of this operation is to introduce anomalies while preserving the rest of the image unchanged.

Prompts are carefully designed to precisely control the generation of anomalies. Each prompt specifies: (i) Defect type: the type of anomaly to introduce (e.g., scratch, crack, stain, dent). (ii) Object type: the object type or surface being modified (e.g., metal plate, plastic part). (iii) Pose and view details: information that ensures the edited image maintains the same camera angle, orientation, and lighting as the original.

# D. Training losses

We train CBMs using the general framework in Sec. III-A. Since both single concept and target predictions are binary classification tasks, we optimize a weighted binary cross-entropy loss, i.e.,  $\mathcal{L}_{C_j} = \mathcal{L}_{\text{BCE}}(c_j, \hat{c}_j, \alpha)$  and  $\mathcal{L}_Y = \mathcal{L}_{\text{BCE}}(y, \hat{y}, \alpha)$ , with:

$$\mathcal{L}_{BCE}(z, \hat{z}; \alpha) = -\frac{1}{n} \sum_{i=1}^{n} (\alpha z^{i} \log \hat{z}^{i} + (1 - z^{i}) \log(1 - \hat{z}^{i})).$$
 (5)

The weight  $\alpha \in \mathbb{R}$  handles the class imbalance present in both the target and concept predictions, since we are in an anomaly detection (AD) setting, and it is computed as the imbalance ratio:

$$\alpha = \frac{\sum_{i=1}^{n} z^{i}}{\sum_{i=1}^{n} 1[z^{i} = 1]} - 1.$$
 (6)

In independent and sequential models, a separate loss is computed for each concept, with  $\alpha$  depending on the imbalance of that specific concept. The individual concept losses are then averaged. For the joint model, the target and concept losses are combined as:

$$\frac{1}{1+\lambda k} \left( \mathcal{L}_Y + \sum_{i=1}^k \mathcal{L}_{\mathcal{C}_i} \right) \tag{7}$$

where k denotes the number of concepts and  $\lambda \in \mathbb{R}$  is the hyperparameter controlling the trade-off between the two objectives.

#### V. EXPERIMENTAL SETTING

#### A. Scenarios

In this work, we provide the results for several scenarios differentiated by the data provided to the CBM model:

**Fully:** trained on both normal and anomalous images (80% of the real anomalous images) from the real dataset.

**Weakly:** we trained the model in a **one-shot per defect type** setting, considering a single anomalous image. This corresponds to 6% of the total anomalies on average.

Weakly(3): contrary to Weakly, it uses three real anomalous images for each defect type, thus considering a **few-shot per defect type** setting. Three anomalous images per defect type correspond to an average of 18% of the anomalous data.

**Synthetic Anomaly Generation (SAG):** It assumes access only to the normal images from the dataset, while anomalous images are generated by a generative model.

**Weakly(3)+SAG:** Weakly(3) scenario but augmented using SAG-generated samples.

**Weakly+SAG:** Weakly scenario but augmented using SAG-generated samples.

#### B. Implementation Details

Models In the Concept Dataset Annotation Pipeline, we mainly leverage Gemma3 [28] as a VLM, except in the Concept Filtering phase, where we use the CLIP ViT-B/32 text encoder [26]. For the text-to-image and image-editing system in the synthetic anomaly generation pipeline, we use the capabilities of Nano Banana, Google's latest image generation model. We train the CBM using MobileNet-v2 as a feature extractor [29] to guarantee efficiency and make our pipeline suitable for resource-constrained settings. To ensure consistency, we report the comparison with PatchCore and STFPM using MobileNet-v2, as reported in a recent study for VAD on edge devices [30].

**Dataset** Our main experimental results are obtained using the MVTecdataset. Further results on additional datasets, including Visa, can be found in the Appendix.

**Hyperparameter Optimization** To select the best hyperparameter configuration, we employ Bayesian optimization, implemented through the Optuna library [31] using the Treestructured Parzen Estimator (TPE) algorithm [32] (see the Appendix for more details).

**Training Details** During training, the CBM model is optimized using the Joint Training paradigm. This approach was selected since it consistently outperforms the other paradigms (ablation study in the Appendix). CBM results are reported as the average performance over three runs with different random seeds. Additional details about training and data augmentation are described in the Appendix.

# C. Metrics

VAD algorithms can be assessed using multiple criteria, corresponding to different levels of analysis:

**Image-level:** To evaluate the model ability to detect abnormalities at the image level, we report the ROC AUC and F1 score, referred to as I-AUC and I-F1, respectively.

**Pixel-level:** To assess performance at the pixel level, we consider three commonly used metrics: ROC AUC, F1 score, and the PRO metric, denoted as P-AUC, P-F1 to avoid ambiguity. **Concept-level:** For Concept Bottleneck Models (CBMs), we evaluate the accuracy of concept predictions using ROC AUC

and F1 score, referred to as C-AUC and C-F1, respectively, to maintain clarity and avoid ambiguity.

Condition	Branch	I-AUC	I-F1	P-AUC	P-F1
CDM Ently	CBM	0.97	0.86	_	-
CBM Fully	Visual	0.96	0.90	0.97	0.50
PatchCore	_	0.96	0.96	0.95	0.48
STFPM	_	0.88	0.93	0.95	0.50

TABLE II: Comparison of image-level (I-AUC/I-F1) and pixel-level (P-AUC/P-F1) performance. The branch column indicates concept-level or visual-level operation.

#### VI. RESULTS

Sec. VI-A compares the performance of the CBM in the fully supervised scenario (upper bound) with the other scenarios: SAG, Weakly, and Weakly+SAG. Sec. VI-B analyzes the pixel-level prediction capabilities of CONVAD in comparison with classic VAD models. Finally, Sec. VI-C assesses the usefulness of the CBM in the VAD setting, particularly to enhance human-machine collaboration.

#### A. CBM Scenarios

A quick comparison of the various CBM scenarios is illustrated in Fig. 1, while a more detailed assessment by category is provided in Table I.

When evaluating the results for the **Fully** scenario in Table I, we immediately notice that the detection performance is notably strong, surpassing that of STFPM. In particular, categories with small and localized anomalies, such as capsule, grid, and screw, show substantial gains under CBM Fully. This improvement aligns with the additional supervision provided in the Fully scenario. The real significant advantage that CBM offers compared to classic VAD approaches like STFPM is the ability to generate concept-based explanations, highlighting the dual strength of CBM in both detection accuracy and interpretable explanations.

Moving to the **Weakly** scenario, where only a single anomalous image per defect type per category is available during training, we observe a considerable performance drop across many categories. This decline is present in both the anomaly detection performance and the concept detection AUC, indicating a correlation between the two metrics. However, the extent of this drop varies significantly by category: for instance, hazelnut and bottle show almost no degradation in anomaly detection performance. On the contrary, categories such as screw and grid experience a severe decline in both tasks.

In the **Weakly+SAG** setting, adding synthetic anomalous images using the SAG procedure to augment the dataset which leads to a substantial average performance gain, particularly in the anomaly detection task. The effect is most pronounced in categories where the unsupervised baseline (STFPM) performs poorly, such as capsule, grid and screw. These categories tend to contain very small anomalous regions, making them harder to distinguish from normal samples [30]. Increasing

the variability of the training distribution through synthetic anomalies helps to compensate for this difficulty: even if the generated defects are suboptimal, they provide a useful signal and raise the baseline in cases where anomalies are intrinsically hard to discriminate.

When examining the **SAG** scenario, where only synthetic anomalies are used during training, we observe contrasting results depending on the category. For instance, categories such as bottle, hazelnut and wood achieve a performance that is slightly lower yet still comparable to the Fully supervised setting. However, several other categories (capsule, metal nut, etc.) experience a more substantial performance drop. These findings suggest that, while SAG is capable of generating visually realistic anomalies, synthetic samples may still diverge from the underlying distributions (and related concepts) observed in real data. This discrepancy likely introduces a distribution shift, which can hinder accurate prediction for certain objects and specific types of defects. Additional plots provided in the Appendix further support this claim.

Fig. 1 shows the average performance for the **Weakly(3)** and **Weakly(3)+SAG** scenarios, confirming the increasing trend in I-AUC when introducing synthetic data augmentation. The results for individual categories are reported in the Appendix.

Finally, we can conclude that (i) the **Fully** CBM is the most interpretable and performs best, although it requires labeled anomalous images (in terms of only defect type). (ii) Generated anomalies can be used effectively to augment a dataset composed of only a few real anomalies, thereby heavily reducing the burden of annotating a large dataset. However, they have limitations when used exclusively as abnormal examples.

#### B. Visual Module

Table II shows a comparison with well-established unsupervised models for VAD. Examining the Visual branch of the CBM Fully, one can see that it achieves higher performance overall with respect to STFPM. Our visual branch is identical to STFPM, but the teacher network is fine-tuned on the concept prediction task, showing the effectiveness of this modification. Notably, through fine-tuning, we inject some domain knowledge into the teacher network, which allows for the extraction of more precise and useful features. With respect to PatchCore, our visual branch obtains similar results; however, it offers concept-based explanations through the CBM branch.

It should be emphasized that the Visual Module is not only valuable for providing intuitive visual explanations to the end user, but it also plays a critical role in ensuring the robustness of the model in the case of failure from the CBM Branch. In addition, since the visual branch of CONVAD relies on STFPM, a method that has been proven effective in identifying never-before-seen data, it should increase **robustness** against previously unseen anomalies, where the CBM may fail.

# C. Intervention

We evaluate the impact of concept-level interventions to assess how manual correction of a few predicted concepts affects model performance (more details about the intervention procedure in the Appendix). Results highlighted in Fig. 4 show that even fixing a small subset of concepts leads to significant improvements in anomaly detection accuracy, confirming the effectiveness of the Concept Bottleneck structure in facilitating human-guided corrections. The obtained results prove the usefulness of CBM in the VAD setting to improve the human-machine collaboration and also high gains in terms of final performance.

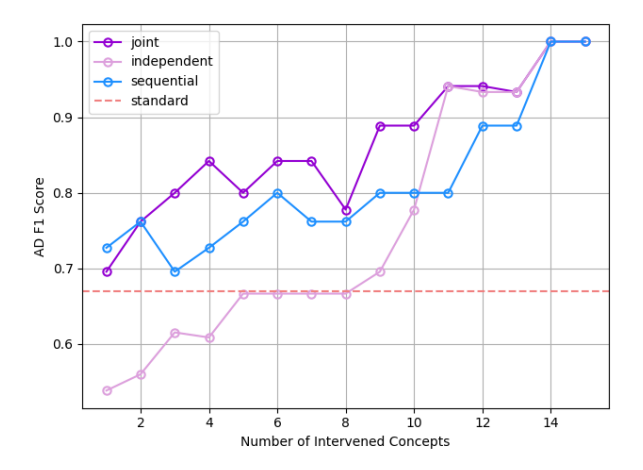


Fig. 4: Gain in performance for the three CBM paradigms while increasing the number of concepts we intervene on, on the *screw* category. The horizontal line indicates the baseline performance training the feature extractor directly to perform anomaly detection, without the concept prediction bottleneck.

# VII. CONCLUSION

In this work, we introduced CONVAD, a novel framework that adapts Concept Bottleneck Models (CBMs) to the Visual Anomaly Detection (VAD) problem. Our approach enables interpretable anomaly detection by learning human-understandable concepts while maintaining competitive performance with traditional VAD models. Through a fully automated concept extraction and annotation pipeline, we demonstrated that meaningful, domain-relevant concepts can be obtained without manual supervision. Moreover, by integrating visual explanations via the student-teacher architecture and introducing a synthetic anomaly generation strategy, CONVAD partially preserves the unsupervised nature of classical VAD approaches.

Our experiments on industrial datasets confirm that CON-VAD achieves strong detection performance, comparable to state-of-the-art baselines, while offering transparent, concept-level reasoning. Importantly, we showed that concept-level interventions, even on a small subset of concepts, yield substantial performance improvements, with the joint training paradigm providing the greatest benefit.

In future work, we plan to test the effectiveness of the Visual Module for novelty detection, i.e., to capture defects that were never seen at training times and thus handle situations where the CBM fails. Finally, we observed that synthetically generated anomalies alone cannot be used to achieve satisfying results, but we believe this is partially due to the pipeline for anomaly generation, which we plan on refining in the future.

#### REFERENCES

- P. Bergmann, M. Fauser, D. Sattlegger, and C. Steger, "Mvtec ad a comprehensive real-world dataset for unsupervised anomaly detection," in 2019 IEEE/CVF Conference on Computer Vision and Pattern Recognition (CVPR), 2019, pp. 9584–9592.
- [2] J. Bao, H. Sun, H. Deng, Y. He, Z. Zhang, and X. Li, "Bmad: Benchmarks for medical anomaly detection," 2024. [Online]. Available: https://arxiv.org/abs/2306.11876
- [3] R. Chan, K. Lis, S. Uhlemeyer, H. Blum, S. Honari, R. Siegwart, P. Fua, M. Salzmann, and M. Rottmann, "Segmentmeifyoucan: A benchmark for anomaly segmentation," 2021. [Online]. Available: https://arxiv.org/abs/2104.14812
- [4] P. W. Koh, T. Nguyen, Y. S. Tang, S. Mussmann, E. Pierson, B. Kim, and P. Liang, "Concept bottleneck models," in *International conference on machine learning*. PMLR, 2020, pp. 5338–5348.
- [5] K. Roth, L. Pemula, J. Zepeda, B. Schölkopf, T. Brox, and P. Gehler, "Towards total recall in industrial anomaly detection," 2022. [Online]. Available: https://arxiv.org/abs/2106.08265
- [6] G. Wang, S. Han, E. Ding, and D. Huang, "Student-teacher feature pyramid matching for anomaly detection," 2021. [Online]. Available: https://arxiv.org/abs/2103.04257
- [7] J. Yu, Y. Zheng, X. Wang, W. Li, Y. Wu, R. Zhao, and L. Wu, "Fastflow: Unsupervised anomaly detection and localization via 2d normalizing flows," arXiv preprint arXiv:2111.07677, 2021.
- [8] T. Defard, A. Setkov, A. Loesch, and R. Audigier, "Padim: a patch distribution modeling framework for anomaly detection and localization," 2020. [Online]. Available: https://arxiv.org/abs/2011.08785
- [9] T. Schlegl, P. Seeböck, S. M. Waldstein, U. Schmidt-Erfurth, and G. Langs, "Unsupervised anomaly detection with generative adversarial networks to guide marker discovery," 2017. [Online]. Available: https://arxiv.org/abs/1703.05921
- [10] T. Schlegl, P. Seeböck, S. M. Waldstein, G. Langs, and U. Schmidt-Erfurth, "f-anogan: Fast unsupervised anomaly detection with generative adversarial networks," *Medical Image Analysis*, vol. 54, pp. 30– 44, 2019. [Online]. Available: https://www.sciencedirect.com/science/ article/pii/S1361841518302640
- [11] Z. You, L. Cui, Y. Shen, K. Yang, X. Lu, Y. Zheng, and X. Le, "A unified model for multi-class anomaly detection," *Advances in Neural Information Processing Systems*, vol. 35, pp. 4571–4584, 2022.
- [12] C.-L. Li, K. Sohn, J. Yoon, and T. Pfister, "Cutpaste: Self-supervised learning for anomaly detection and localization," 2021. [Online]. Available: https://arxiv.org/abs/2104.04015
- [13] V. Zavrtanik, M. Kristan, and D. Skočaj, "Draem-a discriminatively trained reconstruction embedding for surface anomaly detection," in Proceedings of the IEEE/CVF international conference on computer vision, 2021, pp. 8330–8339.
- [14] H. Sun, Y. Cao, H. Dong, and O. Fink, "Unseen visual anomaly generation," in *Proceedings of the Computer Vision and Pattern Recognition Conference*, 2025, pp. 25508–25517.
- [15] P. Wu, X. Zhou, G. Pang, L. Zhou, Q. Yan, P. Wang, and Y. Zhang, "Vadclip: Adapting vision-language models for weakly supervised video anomaly detection," in *Proceedings of the AAAI Conference on Artificial Intelligence*, vol. 38, no. 6, 2024, pp. 6074–6082.
- [16] Z. Gu, B. Zhu, G. Zhu, Y. Chen, M. Tang, and J. Wang, "Anomalygpt: Detecting industrial anomalies using large vision-language models," in Proceedings of the AAAI conference on artificial intelligence, vol. 38, no. 3, 2024, pp. 1932–1940.
- [17] C. Huang, A. Jiang, J. Feng, Y. Zhang, X. Wang, and Y. Wang, "Adapting visual-language models for generalizable anomaly detection in medical images," in *Proceedings of the IEEE/CVF Conference on Computer Vision and Pattern Recognition (CVPR)*, June 2024, pp. 11375–11385.
- [18] J. Choi, J. Raghuram, R. Feng, J. Chen, S. Jha, and A. Prakash, "Concept-based Explanations for Out-of-Distribution Detectors," in Proceedings of the 40th International Conference on Machine Learning. PMLR, Jul. 2023, pp. 5817–5837, iSSN: 2640-3498. [Online]. Available: https://proceedings.mlr.press/v202/choi23e.html
- [19] L. R. Sevyeri, I. Sheth, F. Farahnak, S. E. Kahou, and S. A. Enger, "Transparent Anomaly Detection via Concept-based Explanations," Nov. 2023, arXiv:2310.10702 [cs]. [Online]. Available: http://arxiv.org/abs/2310.10702
- [20] T. Liu, B. Li, X. Du, B. Jiang, X. Jin, L. Jin, and Z. Zhao, "Component-aware anomaly detection framework for adjustable and logical industrial visual inspection," *Advanced Engineering Informatics*, vol. 58, p. 102161, Oct. 2023. [Online]. Available: https://www.sciencedirect.com/science/article/pii/S1474034623002896

- [21] T. Oikarinen, S. Das, L. M. Nguyen, and T.-W. Weng, "Label-free concept bottleneck models," arXiv preprint arXiv:2304.06129, 2023.
- [22] Y. Yang, A. Panagopoulou, S. Zhou, D. Jin, C. Callison-Burch, and M. Yatskar, "Language in a bottle: Language model guided concept bottlenecks for interpretable image classification," in *Proceedings of the IEEE/CVF conference on computer vision and pattern recognition*, 2023, pp. 19187–19197.
- [23] D. Srivastava, G. Yan, and L. Weng, "Vlg-cbm: Training concept bottleneck models with vision-language guidance," *Advances in Neural Information Processing Systems*, vol. 37, pp. 79057–79094, 2024.
- [24] J. Wei, X. Wang, D. Schuurmans, M. Bosma, E. H. Chi, F. Xia, Q. Le, and D. Zhou, "Chain of thought prompting elicits reasoning in large language models," *ArXiv*, vol. abs/2201.11903, 2022. [Online]. Available: https://api.semanticscholar.org/CorpusID:246411621
- [25] T. Brown, B. Mann, N. Ryder, M. Subbiah, J. D. Kaplan, P. Dhariwal, A. Neelakantan, P. Shyam, G. Sastry, A. Askell et al., "Language models are few-shot learners," Advances in neural information processing systems, vol. 33, pp. 1877–1901, 2020.
- [26] A. Radford, J. W. Kim, C. Hallacy, A. Ramesh, G. Goh, S. Agarwal, G. Sastry, A. Askell, P. Mishkin, J. Clark et al., "Learning transferable visual models from natural language supervision," in *International* conference on machine learning. PmLR, 2021, pp. 8748–8763.
- [27] G. Wang, S. Han, E. Ding, and D. Huang, "Student-teacher feature pyramid matching for anomaly detection," arXiv preprint arXiv:2103.04257, 2021.
- [28] G. Team, A. Kamath, J. Ferret, S. Pathak, N. Vieillard, R. Merhej, S. Perrin, T. Matejovicova, A. Ramé, M. Rivière et al., "Gemma 3 technical report," arXiv preprint arXiv:2503.19786, 2025.
- [29] M. Sandler, A. Howard, M. Zhu, A. Zhmoginov, and L.-C. Chen, "Mobilenetv2: Inverted residuals and linear bottlenecks," in *Proceedings* of the IEEE conference on computer vision and pattern recognition, 2018, pp. 4510–4520.
- [30] M. Barusco, F. Borsatti, D. D. Pezze, F. Paissan, E. Farella, and G. A. Susto, "Paste: Improving the efficiency of visual anomaly detection at the edge," in *Proceedings of the Computer Vision and Pattern Recognition Conference*, 2025, pp. 4026–4035.
- [31] T. Akiba, S. Sano, T. Yanase, T. Ohta, and M. Koyama, "Optuna: A next-generation hyperparameter optimization framework," in *Proceedings of the 25th ACM SIGKDD international conference on knowledge discovery & data mining*, 2019, pp. 2623–2631.
- [32] S. Watanabe, "Tree-structured parzen estimator: Understanding its algorithm components and their roles for better empirical performance," arXiv preprint arXiv:2304.11127, 2023.
- [33] Y. Zou, J. Jeong, L. Pemula, D. Zhang, and O. Dabeer, "Spot-the-difference self-supervised pre-training for anomaly detection and segmentation," in *European conference on computer vision*. Springer, 2022, pp. 392–408.
- [34] C. Wang, W. Zhu, B.-B. Gao, Z. Gan, J. Zhang, Z. Gu, S. Qian, M. Chen, and L. Ma, "Real-iad: A real-world multi-view dataset for benchmarking versatile industrial anomaly detection," in *Proceedings of the IEEE/CVF Conference on Computer Vision and Pattern Recognition*, 2024, pp. 22 883–22 892.
- [35] S. Shin, Y. Jo, S. Ahn, and N. Lee, "A closer look at the intervention procedure of concept bottleneck models," in *International Conference* on Machine Learning. PMLR, 2023.

# APPENDIX

## ADDITIONAL EXPERIMENTS

#### A. Weakly(3) Scenario

In Table III we show the supervised scenario using only 3 real anomalous examples per defect type, compared with the same setting, but augmented with the SAG data. We can draw similar considerations to those reported in Section VI-A for the data augmentation effect on the weakly supervised setting.

Category	Weakly(3)		Weakly(3)+SAG	
	C-AUC	I-AUC	C-AUC	I-AUC
Bottle	0.99	1.00	0.78	0.99
Cable	0.82	0.92	0.78	0.91
Capsule	0.70	0.80	0.57	0.62
Carpet	0.60	0.97	0.82	0.96
Grid	0.57	0.58	0.74	0.90
Hazelnut	0.86	1.00	0.83	0.97
Leather	0.77	0.97	0.83	1.00
Metal Nut	0.80	0.70	0.76	0.89
Pill	0.67	0.75	0.72	0.84
Screw	0.62	0.65	0.60	0.81
Tile	0.90	0.99	0.95	0.97
Toothbrush	0.69	0.56	0.82	0.84
Transistor	0.60	0.77	0.64	0.91
Wood	0.89	1.00	0.84	0.99
Zipper	0.90	1.00	0.84	0.97
Average	0.76	0.84	0.76	0.90

TABLE III: Results by category obtained in the Weakly(3) and Weakly(3)+SAG settings over the MVTec-AD categories.

#### B. VisA dataset

In Table IV we report the experiments in the Fully Supervised setting, for all categories of the VisA dataset [33]. The original dataset paper reports PatchCore with a ResNet-50 backbone as the top performer. Despite having an order of magnitude more parameters, it achieves unsupervised performance comparable to CONVAD trained in the Fully Supervised setting with a MobileNet-v2 backbone, illustrating the trade-off between model efficiency and annotation cost.

### C. Real-IAD dataset

In Table V we report the experiments in the Fully Supervised setting, for all categories of the Real-IAD dataset [34]. The I-AUC SimpleNet column reports the best performing model results from the original dataset paper, which confirms the ability of CONVAD to outperform unsupervised methods that require larger model sizes.

## **EVALUATION OF THE CONCEPT ANNOTATION PIPELINE**

To safely guarantee that the proposed pipeline for concept extraction and annotation can be used to produce high-quality results, we evaluate the automatically annotated dataset of the *hazelnut* category against a ground-truth version of it.

Category	C-AUC	I-AUC
Candle	0.89	0.97
Capsules	0.66	0.77
Cashew	0.82	0.97
Chewing Gum	0.91	0.99
Fryum	0.79	1.00
Macaroni 1	0.62	0.96
Macaroni 2	0.71	0.95
PCB1	0.76	0.97
PCB2	0.69	0.81
PCB3	0.70	0.93
PCB4	0.72	1.00
Pipe Fryum	0.83	0.99
Average	0.76	0.94
Average (PatchCore)	-	0.93

TABLE IV: Results obtained on the **Visa Dataset** in the Fully Supervised setting.

Specifically, we compute accuracy, precision and recall of the predicted concepts. Table VI displays a summary of our findings. Overall, predicted concepts can be considered of good quality, especially those that appear more often in normal images; as for anomalous concepts, we observe a very high variability in terms of precision and recall, which is mainly related to those concepts that describe a diffused feature of the image (e.g., *surface discontinuity, uneven tone, etc.*), which are more difficult to capture for a VLM and can be arbitrary for a domain expert as well.

#### ADDITIONAL TRAINING DETAILS

Each model is trained for a maximum of 100 epochs, with an early stopping mechanism triggered after ten epochs. When performance reaches a plateau after five epochs, we also allow the learning rate to be reduced by a factor of 10.

Transformation-based data Augmentation. We apply transformations to enhance the model generalization ability, carefully choosing those that preserve the presence of each concept, ensuring the integrity of attribute labels. The transformations applied are the following: horizontal and vertical flips with probability 0.5, random rotation by a 25-degree angle, brightness jitter by a factor of 0.2, and contrast jitter by a factor of 0.2.

**CBM Training.** We attach k parallel linear layers to the CNN feature extractor, that act as concept predictors, while a simple Feed-Forward Neural Network with eight neurons is employed for anomaly detection. The feature extractor undergoes a pretraining phase directly on the dataset of interest, in which it is optimized according to a multi-class classification objective to learn which object is depicted in the image, while its last layers are fine-tuned during training for the concept prediction task.

#### **CBM TRAINING MODALITIES**

Table VII displays a comparison of the results obtained by the three CBM paradigms on MVTec-AD. In consideration

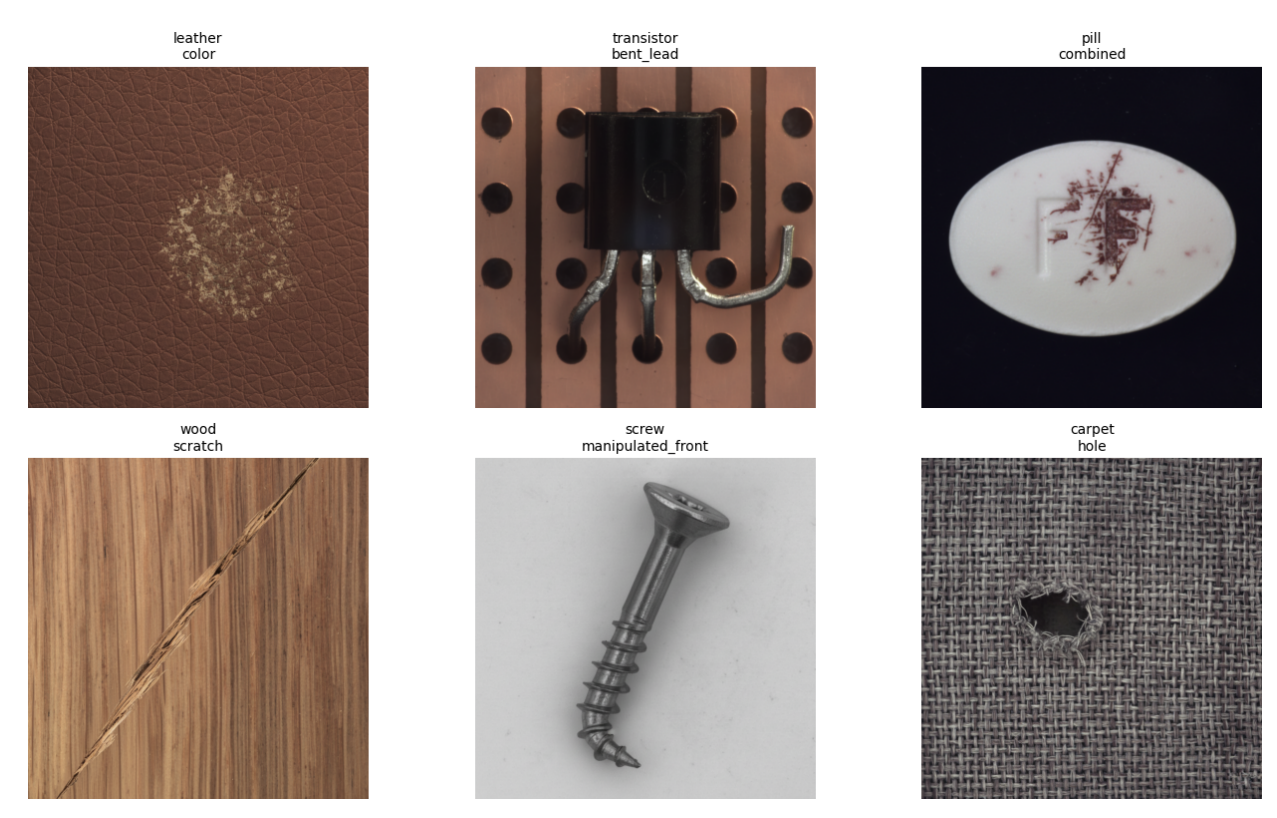


Fig. 5: Examples of well-generated synthetic anomalous images.

of these findings, the CBM model is trained using the Joint paradigm, unless stated otherwise in the paper, since it performs the best on three of the four evaluated metrics.

#### INTERVENTION PROCEDURE

In Section VI-C, we demonstrate the impact on performance of manually modifying predicted concepts with their ground-truth value during inference. However, this procedure can be costly, as it requires the supervision of a human expert, so several strategies have been devised to minimize such costs by focusing first on the concepts that should be more important to provide an increase in performance. We followed the UCP (Uncertain Concept Prediction) heuristic proposed in [35] and computed the entropy-based uncertainty related to each concept prediction:

$$\mathcal{H}(c_i) = -(p_i \cdot \log(p_i) + (1 - p_i) \cdot \log(1 - p_i)). \tag{8}$$

We then sorted the entropy scores in descending order, following the idea that concepts predicted with more uncertainty might confuse the model and lead to incorrect predictions. As mentioned in III, since the joint model uses the predicted concept logits to perform the main task, we substitute them with either the 5th or the 95th percentile of the training distribution.

## CONCEPT LOGITS ANALYSIS

In the SAG column of Table I, where the model is trained exclusively on generated anomalies and evaluated on real ones, some categories achieve high concept-level AUC (C-AUC) and image-level AUC (I-AUC), while others fail to transfer

effectively to real data. Two extreme examples illustrating this contrast are hazelnut, which transfers well, and metal nut, which does not. We examine the concept-logit embeddings extracted from the training and test examples to investigate this discrepancy. The test set contains only real normal and real anomalous examples, while the training set may include synthetic images in the SAG scenarios. Some examples of the synthetic pictures obtained (and used in the SAG scenarios) can be found in Fig. 5. All models compared within each category use the same random seed, training data, and evaluation set, with the latter containing only real anomalies that were not used for weak supervision in any of the models.

A well-learned bottleneck should ensure (i) a separation between normal and anomalous samples, provided that the concept set is sufficiently predictive, and (ii) tight clustering of images sharing the same or similar defect type (e.g., "hole" or "crack" in hazelnut). Moreover, if the synthetic anomalies are sufficiently well aligned with the real anomaly domain, their concept-logit representations should be consistent with those of real anomalies, indicating an effective transfer. To obtain qualitative insights about these aspects, we plot 2-dimensional t-SNE visualizations of the concept logits.

In the hazelnut SAG scenario, we obtain an average C-AUC of 0.89 and an I-AUC of 0.99. Figure 6, shows a clear separation between Train Normal samples and Train Anomalous (synthetic). Test Normal samples appear in the same region as Train Normal, which is expected since their domains match, as both correspond to real images. In addition, Test Anomalous (real images) are mapped to the same broad regions as synthetic anomalies (Train

Category	C-AUC	I-AUC	I-AUC SimpleNet
Audiojack	0.82	0.90	0.88
Bottle Cap	0.85	0.96	0.95
Button Battery	0.89	0.95	0.88
End Cap	0.88	0.92	0.81
Eraser	0.94	0.97	0.93
Fire Hood	0.78	0.87	0.95
Mint	0.68	0.85	0.69
Mounts	0.89	0.96	0.95
PCB	0.87	0.94	0.92
Phone Battery	0.80	0.86	0.93
Plastic Nut	0.92	0.94	0.86
Plastic Plug	0.81	0.89	0.94
Porcelain Doll	0.90	0.98	0.87
Regulator	0.87	0.89	0.98
Rolled Strip Base	0.95	1.00	1.00
Sim Card Set	0.90	1.00	0.99
Switch	0.90	0.96	0.97
Tape	0.93	0.98	0.99
Terminal Block	0.93	0.97	0.99
Toothbrush	0.90	0.98	0.91
Toy	0.93	0.96	0.91
Toy Brick	0.90	0.93	0.84
Transistor 1	0.88	0.99	0.98
U-Block	0.87	0.93	0.93
USB	0.81	0.95	0.97
USB Adaptor	0.80	0.94	0.87
VC Pill	0.96	1.00	0.92
Wooden Beads	0.92	0.93	0.85
Woodstick	0.92	0.96	0.86
Zipper	0.97	1.00	1.00
Average	0.88	0.94	0.92

TABLE V: Results obtained on the **Real-IAD Dataset** in the Fully Supervised setting. We considered single-view Real-IAD, keeping only the view with the highest number of anomalies in each category.

	All	<b>Anomaly Concepts</b>	<b>Normal Concepts</b>
Acc	$0.93 \pm 0.08$	$0.92\pm0.08$	$0.98\pm0.01$
Prec	$0.76\pm0.24$	$0.71\pm0.23$	$0.99\pm0.00$
Rec	$0.77 \pm 0.28$	$0.72\pm0.28$	$0.99 \pm 0.01$

TABLE VI: Average value and standard deviation of accuracy, precision and recall of predicted concepts over the *hazelnut* category.

Model type	C-AUC	C-F1	I-AUC	I-F1
Joint	0.86	0.76	0.97	0.86
Sequential	0.85	0.75	0.95	0.85
Independent	0.87	0.72	0.96	0.85

TABLE VII: Comparison of the results of the three CBM learning paradigms over the MVTec-AD dataset, in terms of concept prediction performance and anomaly detection.

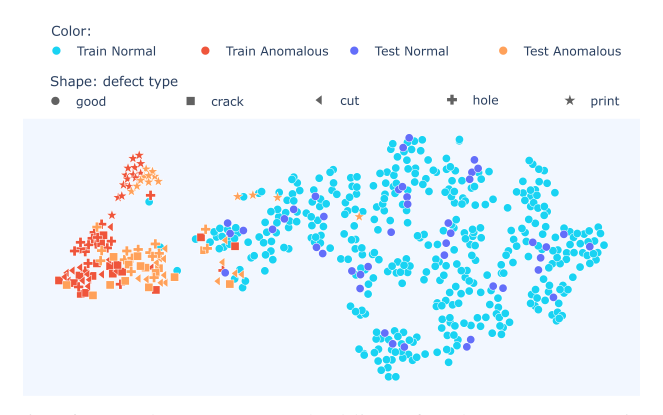
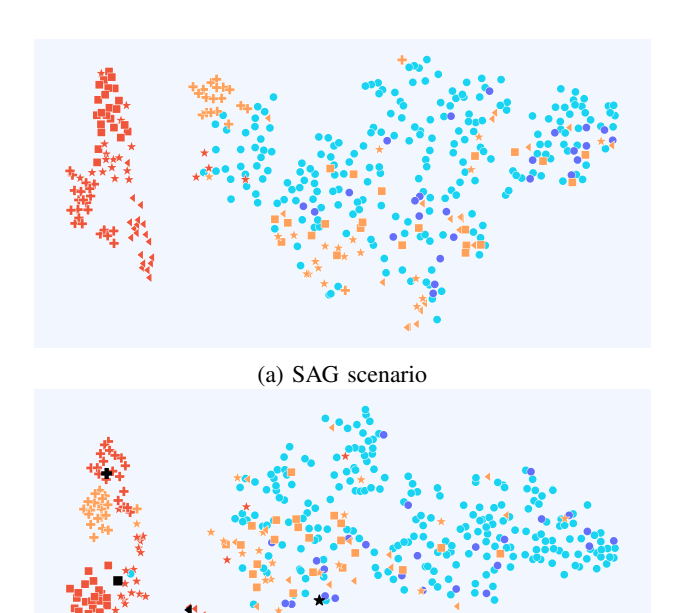


Fig. 6: Hazelnut t-SNE embeddings for the SAG scenario.

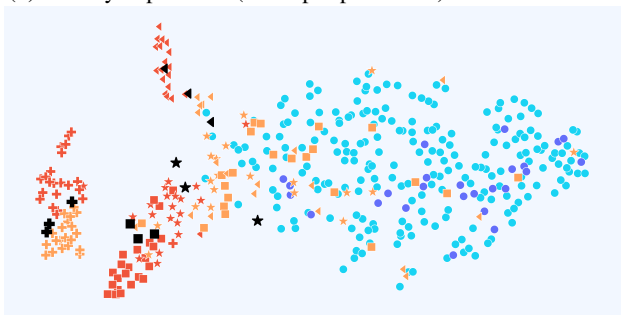
Anomalous), which is ideal. Within this anomalous region, the "print" defect forms a distinct sub-cluster, while "crack", "cut" and "hole" share more overlapping embeddings, reflecting their visual similarity. These patterns are consistent with the high AUC scores and indicate that the synthetic anomalies generated for the hazelnut category effectively capture relevant characteristics of real anomalies.

However, for the metal nut in the SAG scenario, the C-AUC drops to an average of 0.59, and the I-AUC drops to 0.66. In this case, in Figure 7(a), most Test Anomalous (real) samples are located within regions corresponding to Train Normal and Test Normal data, rather than being mapped near the synthetic Train Anomalous samples. Only the "flip" defect forms a slightly separated cluster (due to its visual dissimilarity to other images), while other defects are scattered among normal samples. This qualitative mismatch between synthetic and real anomaly embeddings explains the degraded AUCs and suggests poorly generated anomalies.

Exploring the embeddings in the Weakly+SAG scenarios provides a deeper understanding of why introducing even a small number of real anomalies, combined with synthetic anomalies, reduces this discrepancy in performance. For the metal nut in the Weakly+SAG scenario (adding one real anomaly per defect type in training), the C-AUC improves to an average of 0.70 and the I-AUC to 0.84, and Figure 7(b) shows a closer alignment between synthetic and real anomalies. With Weakly(3)+SAG (three real anomalies per type), the C-AUC increases to 0.76 and the I-AUC to 0.89. Simultaneously, the representations of real anomalies appear closer to those of synthetic ones, and clusters associated with different defect types become more clearly separated (Figure 7(c)). These results indicate that when using synthetic anomalies for training, even minimal real-data supervision can



(b) Weakly supervised (1 sample per defect) + SAG scenario.



(c) Weakly supervised (3 samples per defect) + SAG scenario.



Fig. 7: t-SNE representations of concept logits embeddings using metal\_nut. Black markers highlight the few real samples used for Weakly+SAG scenarios.

mitigate the domain shift and encourage the concept space to encode a more consistent defect-specific structure, eliminating the need to collect a large dataset of rare and difficult-to-acquire anomalies.